

*The combined influence of the stratospheric polar vortex and ENSO on zonal asymmetries in the Southern Hemisphere upper tropospheric circulation during austral spring and summer*

Article

Supplemental Material

Osman, M., Shepherd, T. G. ORCID: <https://orcid.org/0000-0002-6631-9968> and Vera, C. S. (2022) The combined influence of the stratospheric polar vortex and ENSO on zonal asymmetries in the Southern Hemisphere upper tropospheric circulation during austral spring and summer. *Climate Dynamics*, 59 (9-10). pp. 2949-2964. ISSN 1432-0894 doi: 10.1007/s00382-022-06225-0 Available at <https://centaur.reading.ac.uk/104127/>

It is advisable to refer to the publisher's version if you intend to cite from the work. See [Guidance on citing](#).

To link to this article DOI: <http://dx.doi.org/10.1007/s00382-022-06225-0>

Publisher: Springer

including copyright law. Copyright and IPR is retained by the creators or other copyright holders. Terms and conditions for use of this material are defined in the [End User Agreement](#).

[www.reading.ac.uk/centaur](http://www.reading.ac.uk/centaur)

## **CentAUR**

Central Archive at the University of Reading

Reading's research outputs online

1 The Combined Influence of the Stratospheric Polar Vortex and  
2 ENSO on Zonal Asymmetries in the Southern Hemisphere Upper  
3 Tropospheric Circulation during Austral Spring and Summer:  
4 Supplementary material

5 Marisol Osman

Theodore G. Shepherd

Carolina S. Vera

6 April 26, 2021

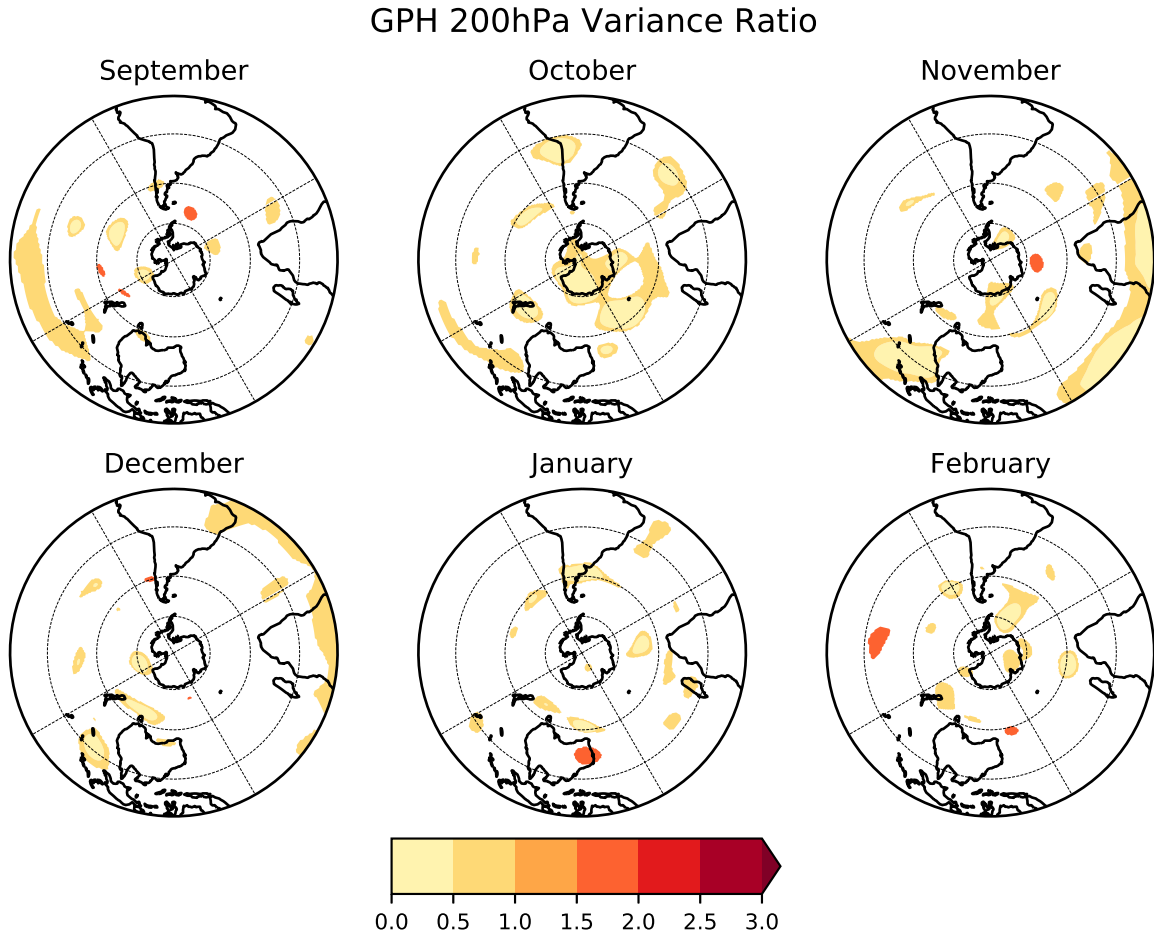


Figure S1: Ratio of climatological variance of  $Z$  at 200hPa between hindcasts and ERA-Interim for (a) September, (b) October, (c) November, (d) December, (e) January, (f) February 1981-2018. The year 2002 has been excluded. Coloured regions indicate differences that are statistically different at the 5% level based on a two-sided chi-square test. Hindcasts initialized on 1 August.

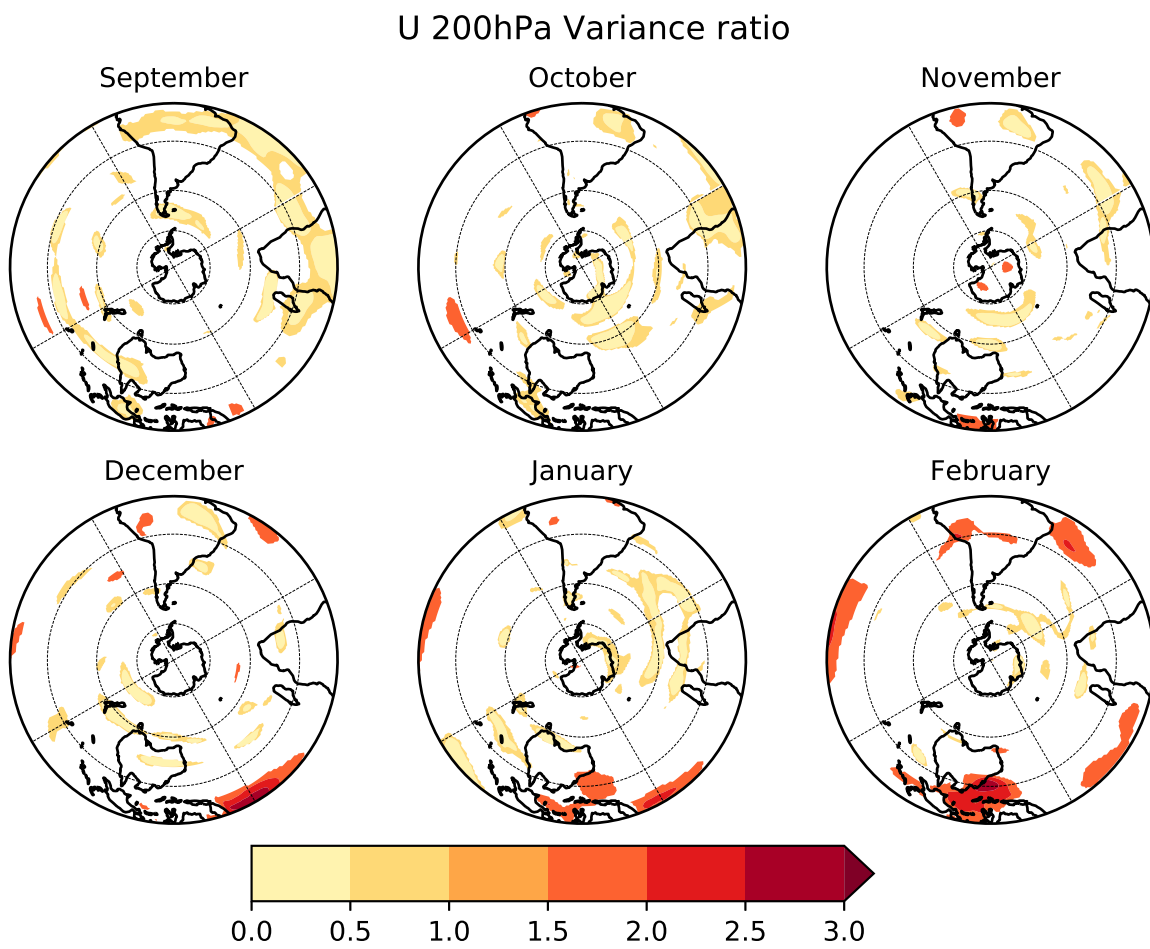


Figure S2: Same as Fig. S1 but for zonal wind  $u$ .

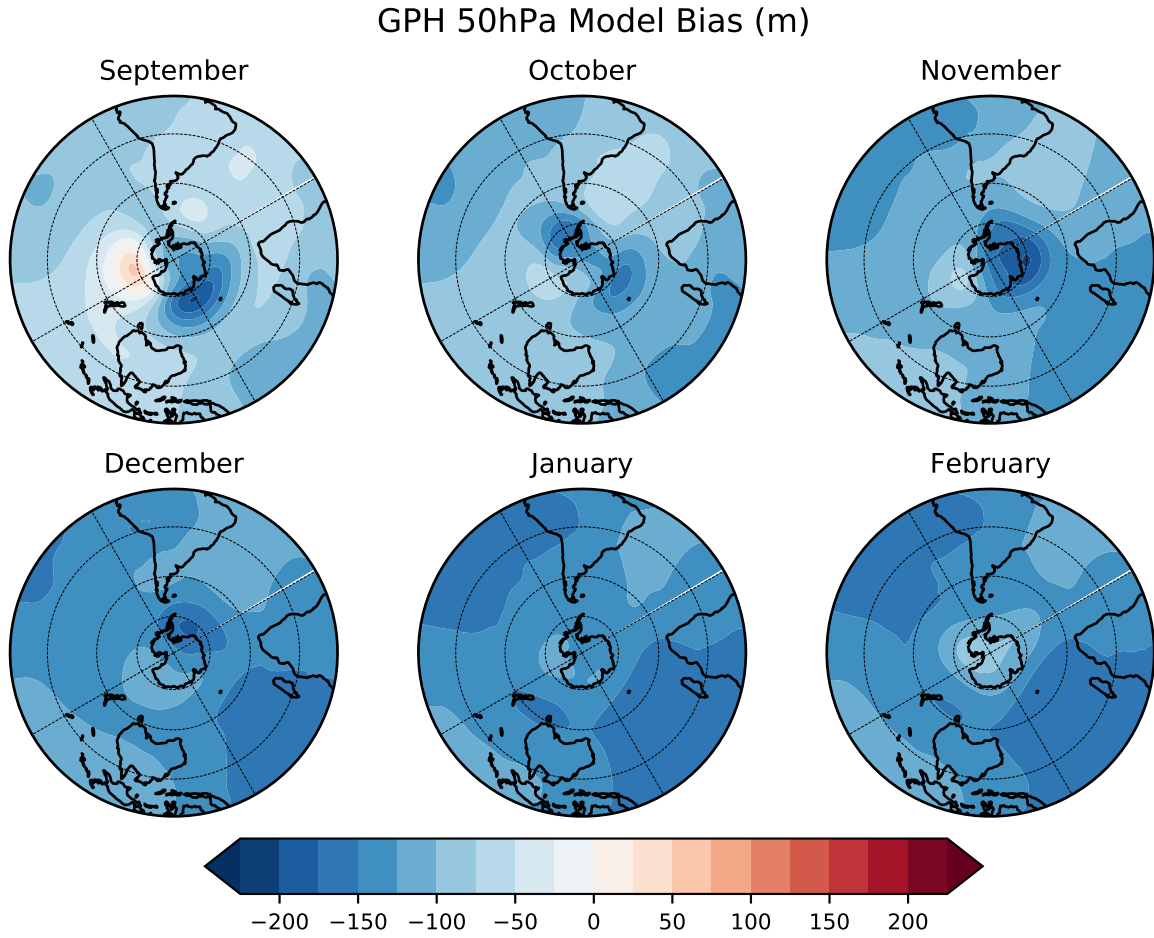


Figure S3: Monthly mean climatological differences in  $Z$  at 50hPa between hindcasts and ERA-Interim (m) for (a) September, (b) October, (c) November, (d) December, (e) January, (f) February 1981-2018. The year 2002 has been excluded. Coloured regions indicate differences that are statistically different at the 5% level based on a two-sided t-test. Hindcasts initialized on 1 August.

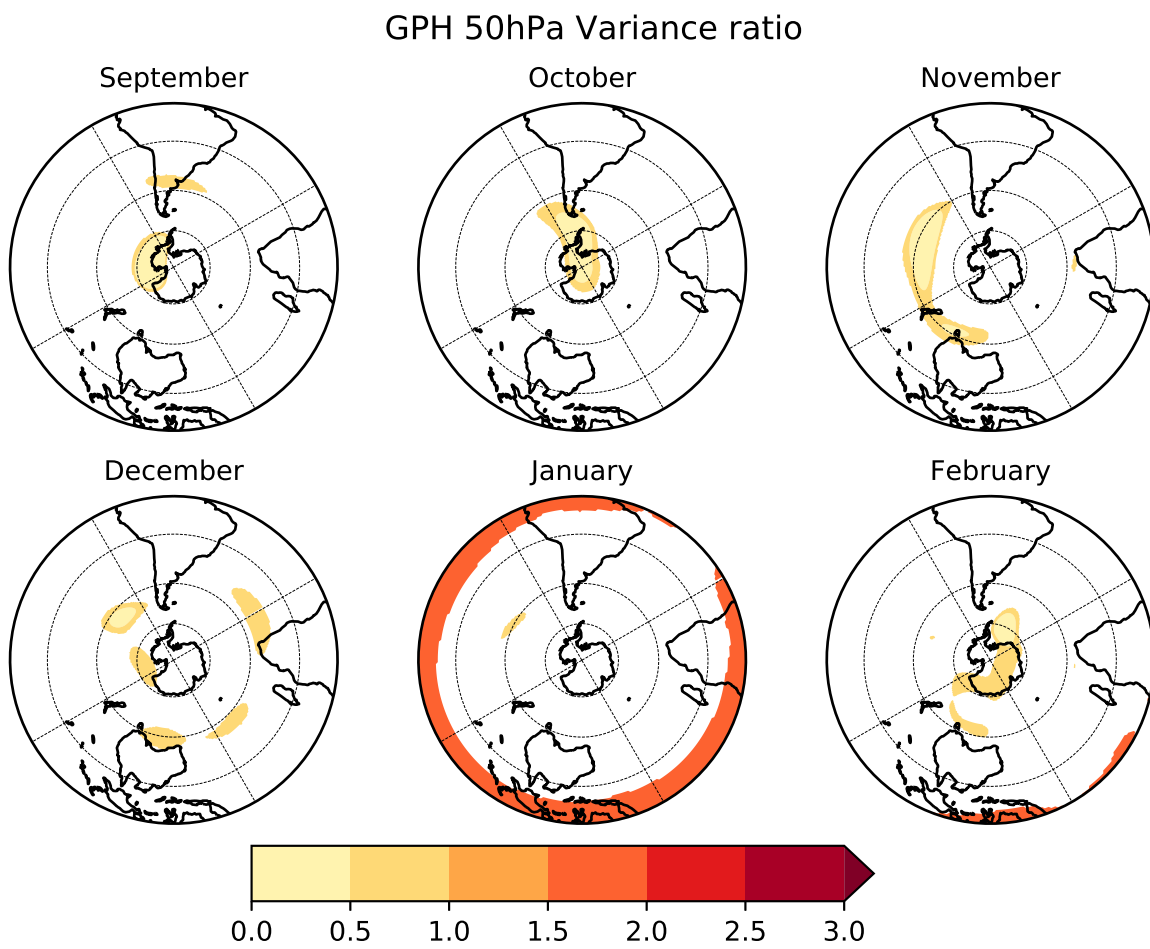


Figure S4: Same as Fig. S1 but for  $Z$  at 50hPa.

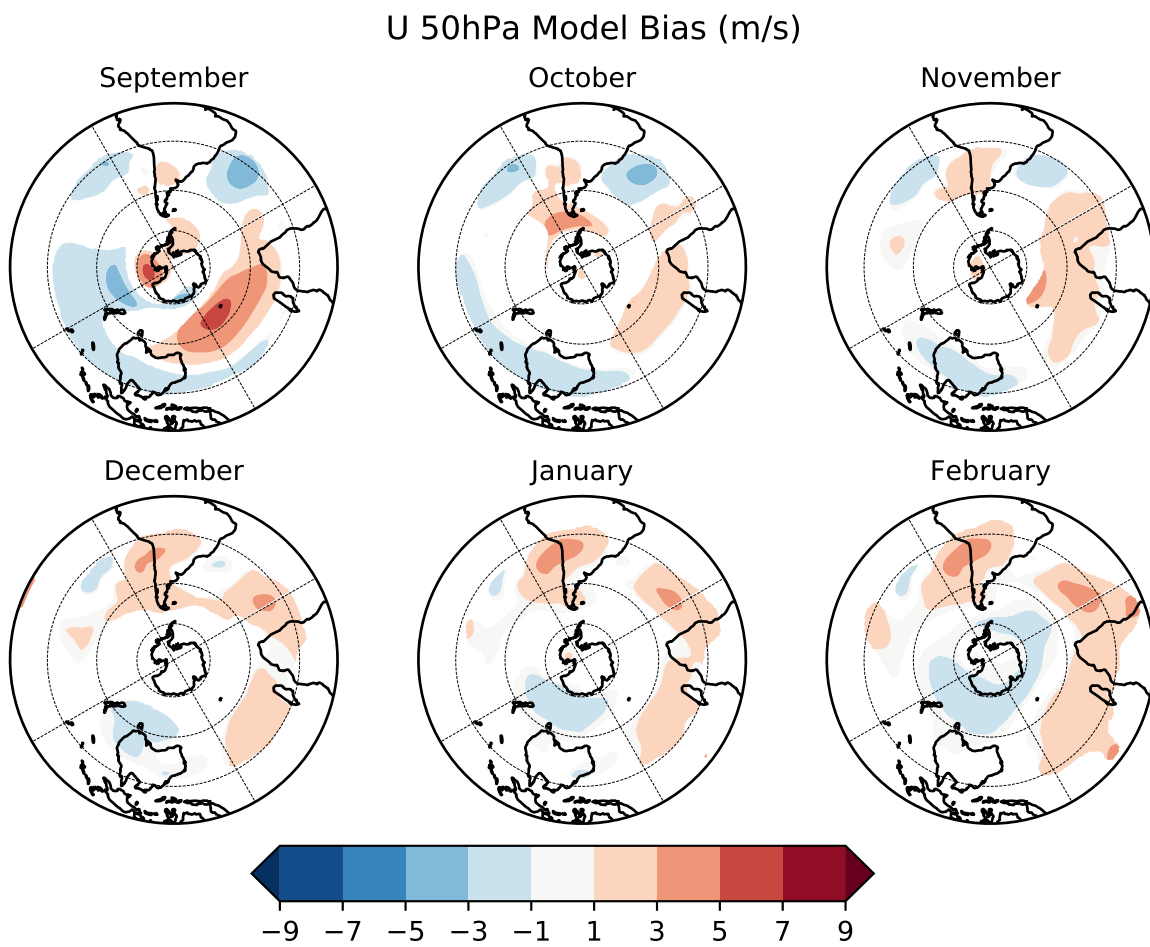


Figure S5: Same as Fig. S3 but for zonal wind  $u$ .

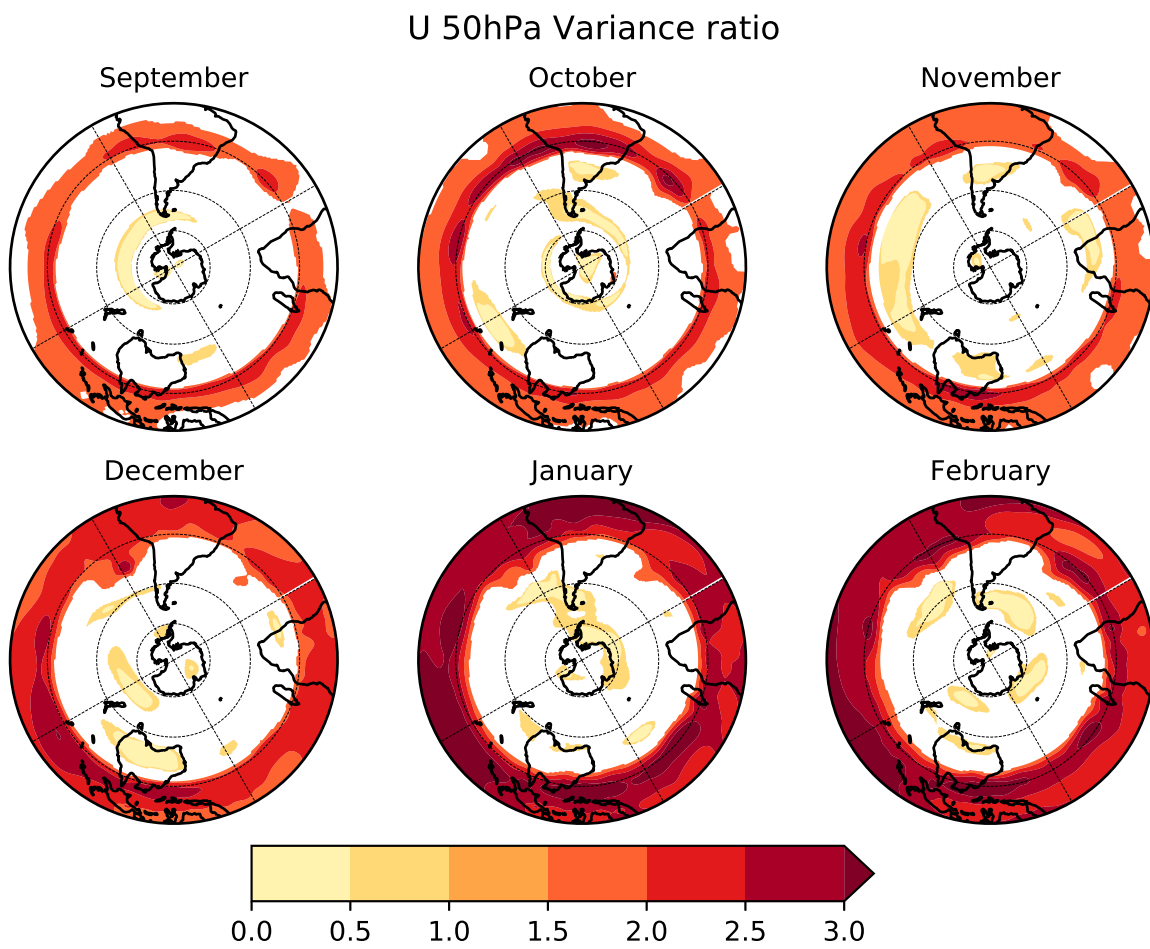


Figure S6: Same as Fig. S2 but for zonal wind  $u$  at 50hPa.

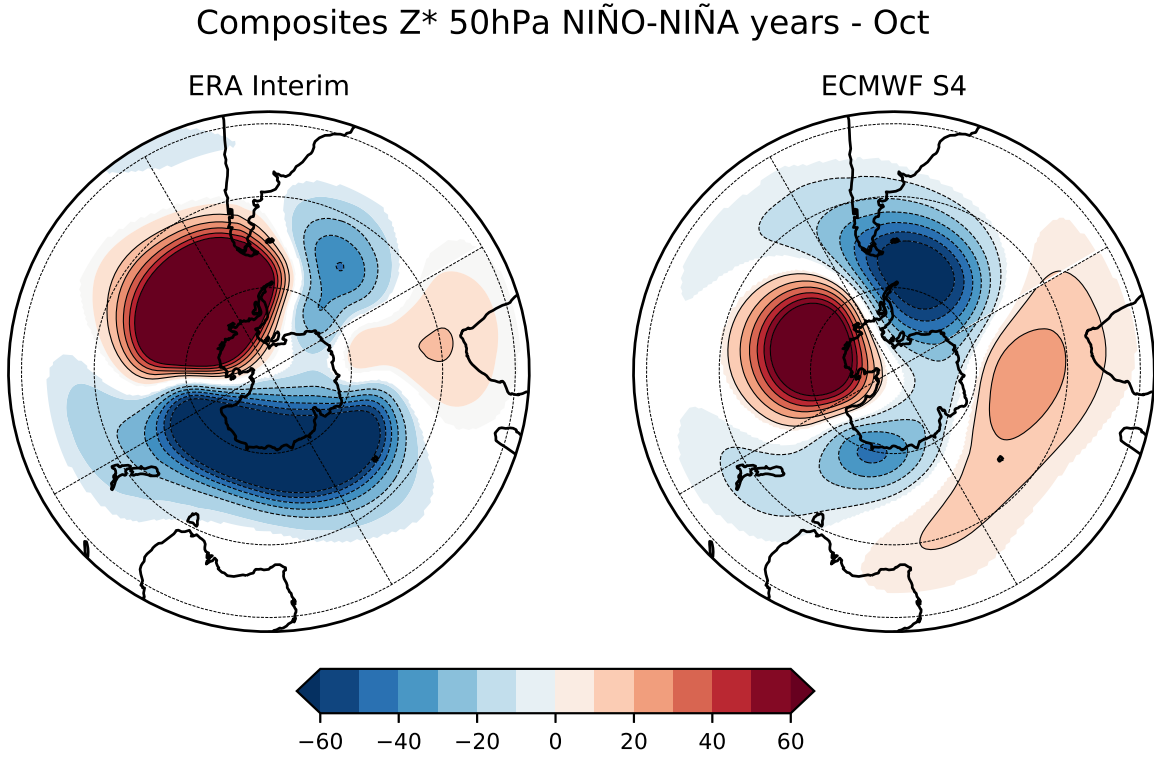


Figure S7: Composite differences of  $Z^*$  at 50hPa between El Niño and La Niña in October for (a) ERA-Interim and (b) hindcasts. Units are in m and coloured regions are statistically different from zero at the 5% level based on a t-test.

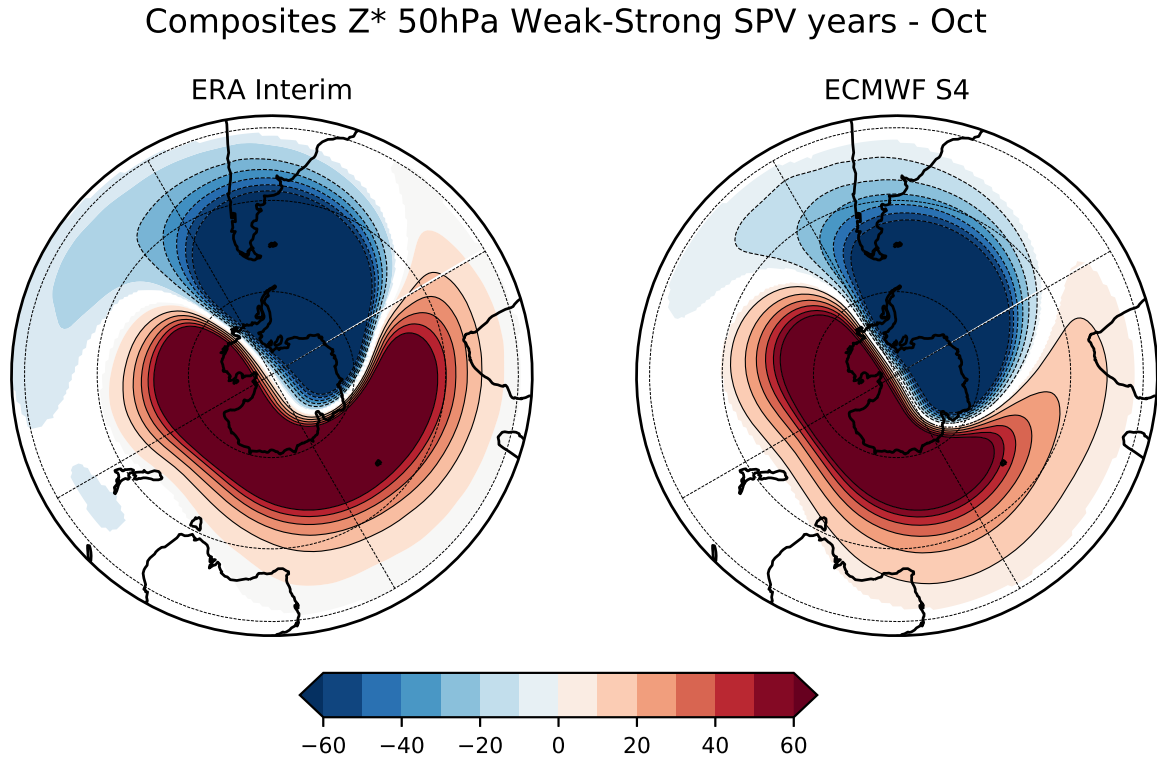


Figure S8: Composite differences of  $Z^*$  at 50hPa between weak and strong SPV in October for (a) ERA-Interim and (b) hindcasts. Units are in m and coloured regions are statistically different from zero at the 5% level based on a t-test.

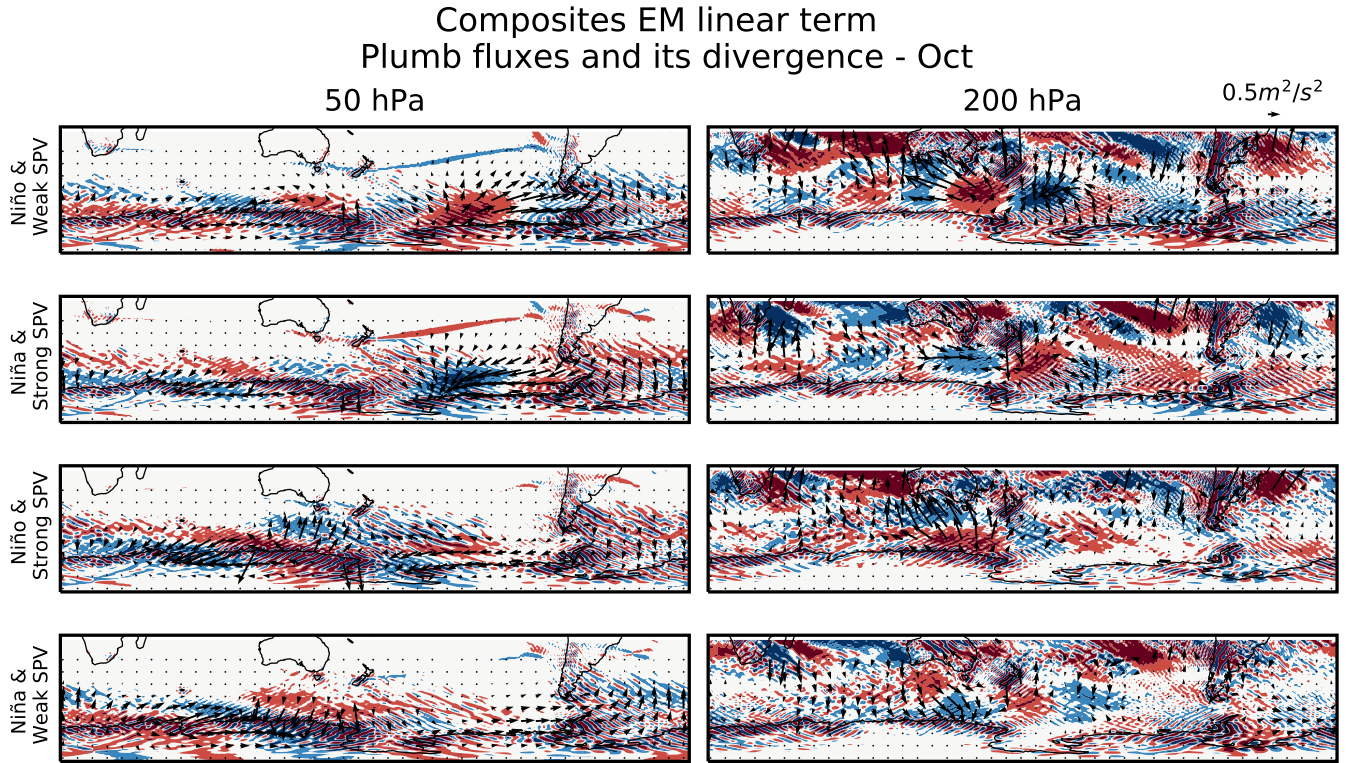


Figure S9: Linear term of the ensemble mean response of the wave activity flux response (arrows) and its divergence (shaded) at 50hPa (left column) and 200hPa (right column) to in-phase and out-of-phase events. Convergence (divergence) levels are  $\pm 0.3e-6ms^{-2}$  and  $\pm 1e-6ms^{-2}$ .

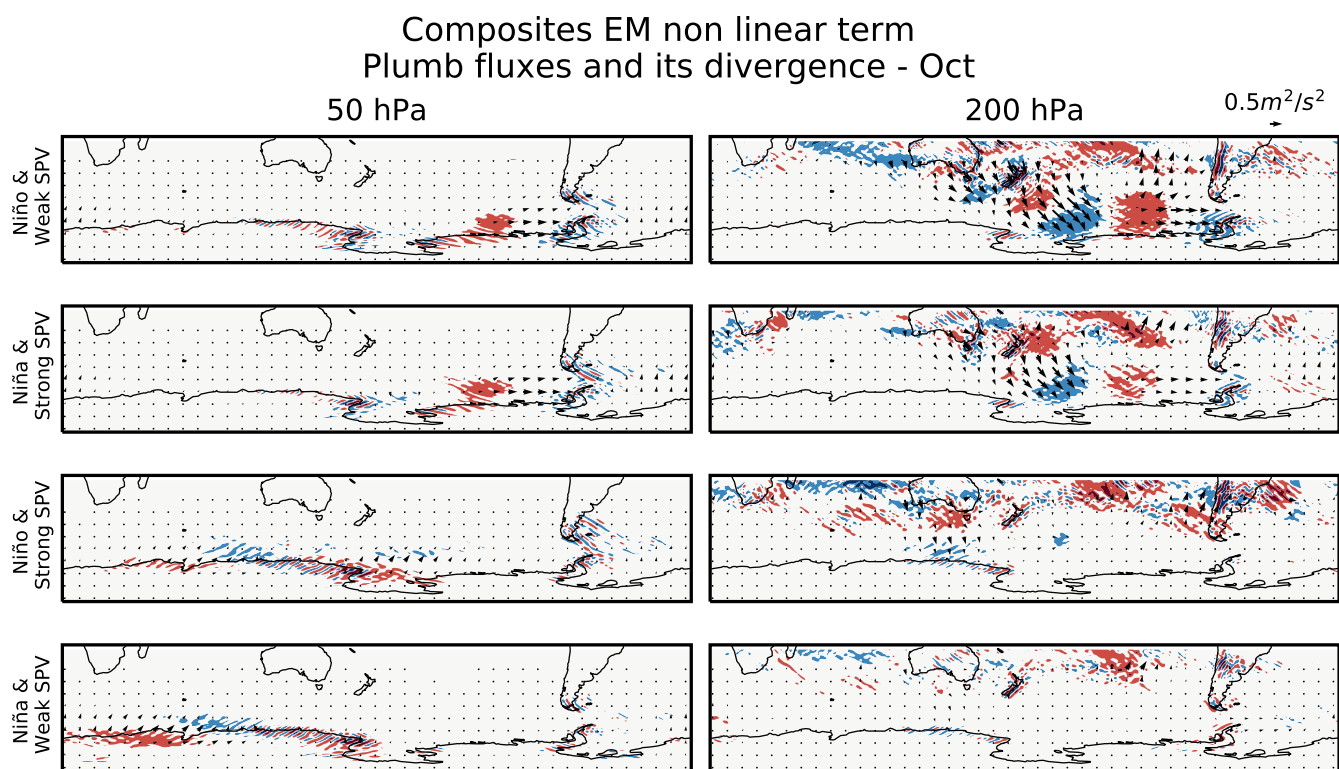


Figure S10: Same as Fig. S9 but for the non-linear term of the ensemble mean response.